

## Thiadiazoles as Corrosion Inhibitors for Carbon Steel in H<sub>2</sub>SO<sub>4</sub> Solutions

Octavio Olivares-Xometl<sup>1,\*</sup>, Natalya V. Likhanova<sup>2</sup>, Noel Nava<sup>2</sup>, Agustín Cabral Prieto<sup>3</sup>, Irina V. Lijanová<sup>4</sup>, A. Escobedo-Morales<sup>1</sup>, Claudia López-Aguilar<sup>1</sup>

<sup>1</sup> Benemérita Universidad Autónoma de Puebla, Facultad de Ingeniería Química, Av. San Claudio y 18 sur, Col. San Manuel, Ciudad Universitaria, Puebla, 72570, México.

<sup>2</sup> Instituto Mexicano del Petróleo, Programa de Investigación y Posgrado, Eje Central Lázaro Cárdenas No. 152, Col. San Bartolo Atepehuacan, México, 07730, DF.

<sup>3</sup> Instituto Nacional de Investigaciones Nucleares, Departamento de Química, Carretera México-Toluca S/N, la Marquesa, Ocoyoacac, 52750, México.

<sup>4</sup> Instituto Politécnico Nacional, CIITEC, Cerrada Cecati S/N, Colonia Santa Catarina, Azcapotzalco, 02250, México, DF.

\*E-mail: [oxoctavio@yahoo.com.mx](mailto:oxoctavio@yahoo.com.mx)

Received: 18 September 2012 / Accepted: 29 November 2012 / Published: 1 January 2013

---

Six organic compounds derived from 2-amino-5-alkylthiadiazole were evaluated as corrosion inhibitors of carbon steel 1018 (CS 1018) in 1.0 M H<sub>2</sub>SO<sub>4</sub>. The inhibition efficiency displayed by the synthesized compounds was assessed by mass loss, using a concentration interval of 10-100 ppm at 25 and 40 °C. The potentiodynamic tests were carried out only with the compounds that showed the lowest [AMT], intermediate [AHT] and highest [ATT] inhibition efficiencies obtained by mass loss. The inhibition efficiency results obtained by both techniques showed that the length of the alkylic chain in this kind of compounds plays a major role in their optimum performance as corrosion inhibitors. In addition, from the analysis of the calculated electrochemical parameters, it was found that the evaluated compounds present properties of mixed-type inhibitors. As for the adsorption mechanism on the CS 1018 metal surface in 1.0 M H<sub>2</sub>SO<sub>4</sub>, it was found to be of physical type. The characterization of the corrosion products formed on CS has been carried out by <sup>57</sup>Fe Mössbauer spectroscopy. The major constituent of the rust formed in this environment in the presence of 2-amino-5-alkylthiadiazole is Szomolnokite.

---

**Keywords:** acid medium; corrosion inhibitor; inhibition efficiency; thiadiazole

### 1. INTRODUCTION

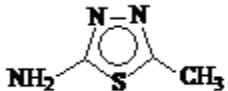



Different types of metals and alloys are frequently used in the heavy industry. Carbon steel (CS) is, for example, employed in the construction of tanks, heat exchangers, distillation towers,

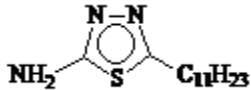
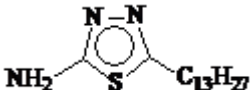
drums, pipelines, etc. In most cases, these CS containers are subjected during their operation to environmental compounds such as salts, inorganic compounds, gases, etc., which may cause corrosion on them [1, 2]. Thus, corrosion studies of CS containers in corrosive aqueous phase media are of considerable interest due to their common occurrence, for example, in the chemical and petrochemical industries [3, 4]. There are many available chemical methods to prevent corrosion on those containers subjected to aggressive environments. The use of corrosion inhibitors is one of these methods and could be considered as one of the most economic [2, 3, 5]. Numerous organic inhibitors have been used in this area, for instance, imidazolines, primary amines, diamines, aminoamines, oxyalkylated amines, fatty acids, naphthanic acid, phosphate esters and dodecylbenzenesulfonic acids, among others [6]. Particularly, thiadiazole (TDZ) compounds have arisen much interest as corrosion inhibitors lately [7-11], due to their wide inhibition efficiency, which is modified by changing their substitution groups [12-14]. Their use for the protection of a variety of metal/alloys in acid medium is getting wide [15-19]. Present results show an inhibition efficiency of TDZ compounds that range from 23 to 97% by changing their available substitution groups. Hence, the chemical activity of these TDZs is organic-structure-dependent, defining in this way their physico-chemical properties of adsorption on metal surfaces [12-19]. In this context, the aim of this work is to investigate the behavior of the aliphatic chain (fifth position) with the same amino "bound" group (second position) in the structure of TDZ molecules as corrosion inhibitors on CS. All different TDZ molecules were evaluated as corrosion inhibitors on CS 1018 by the weight loss and potentiodynamic techniques. The corrosion products were analyzed by X-ray diffraction (XRD) and Mössbauer Spectroscopy (MS) in the absence and presence of corrosion inhibitors.

## 2. EXPERIMENTAL WORK

### 2.1 Test solution

**Table 1.** Structure and name of the compounds evaluated as corrosion inhibitors en 1.0 M H<sub>2</sub>SO<sub>4</sub> for CS 1018.

Structure	Name/Entry	Relative Molecular weight
	2-Amino-5-methyl-1,3,4-thiadiazole (AMT)	115.15
	2-Amino-5-ethyl-1,3,4-thiadiazole (AET)	129.18
	2-Amino-5-n-propyl-1,3,4-thiadiazole (APrT)	143.21
	2-Amino-5-heptyl-1,3,4-thiadiazole (AHT)	199.31

	2-Amino-5-undecyl-1,3,4-thiadiazole (AUT)	255.42
	2-Amino-5-tridecyl-1,3,4-thiadiazole (ATT)	283.48

A test solution was prepared by using standard grade sulfuric acid and deionized water. An aqueous solution of 1.0 M sulfuric acid was used as the corrosive medium. Table 1 shows the chemical names and acronyms of the TDZ molecules used in the present work. Each selected TDZ compound was added to the aqueous test solution, using 10, 25, 50, 80 and 100 ppm concentrations.

## 2.2 Weight loss tests

The weight loss tests were performed on the metallic samples of CS 1018 with dimensions of 1.5 cm x 1.5 cm x 0.0254 cm. Before using these samples, they were wet abraded with silicon carbide paper from number 200 to 2000 grit, degreased with hexane and rinsed in isopropanol and acetone. The clean metallic samples were placed in an oven at 100 °C for 2 h, drying them completely before weighing. For each experiment, three cleaned samples were immersed in the aqueous test solution at temperatures of 25 and 40 °C for 7 h, respectively. The metallic samples were then removed from the aqueous solution, washed, dried and placed in a desiccator before their final weight loss test.

## 2.3 Electrochemical tests

Electrochemical tests were performed in a conventional three-electrode glass cell. Electrode potential was measured against a saturated calomel electrode (SCE) via a Luggin capillary probe, which was used as the reference electrode. The counter electrode was a Pt mesh (99.9% purity), and the working electrode was a CS 1018 sample with a surface area of 3.16 cm<sup>2</sup>. Before testing, the working electrodes were polished (200 to 2000 grit), cleaned in ethanol, and dried in a flux of high purity nitrogen. The electrochemical measurements were performed in the test solution at 25 ± 1 °C after reaching the open-circuit potential ( $E_{ocp}$ ). Electrochemical tests were performed in a PGSTAT302N potentiostat/galvanostat controlled by a PC through the General Purpose Electrochemical System (GPES). The polarization curves were performed in the potential range of ± 250 mV against the  $E_{ocp}$  at a scan rate of 0.166 mVs<sup>-1</sup>. The cathodic region was scanned from -250 mV to the  $E_{ocp}$ , whereas the anodic region was scanned from  $E_{ocp}$  to +250 mV, both at the same scan rate.

## 2.4 Corrosion product analysis

The CS 1018 (C-0.17%, Mn-0.40%, P-0.040%, S-0.050%, Fe balance, wt.%) samples were exposed to 100 mL of 1.0 M H<sub>2</sub>SO<sub>4</sub> for two months at 25 ± 1 °C, using 100 ppm of corrosion

inhibitors; the corrosion products were then brushed from steel surface to collect a few milligrams to be analyzed by XRD and Mössbauer spectroscopy. X-ray patterns were obtained in a Siemens D500 diffractometer equipped with a copper anode X-ray tube; the  $K\alpha$  radiation ( $\lambda = 1.5405 \text{ \AA}$ ) was selected with a diffracted beam monochromator, covering a diffraction angle range of  $2\theta$  from 4 to 70 in  $0.03^\circ$  increments.

Mössbauer spectra were recorded at 300 and 77 K, using a conventional constant acceleration Mössbauer spectrometer, operated in transmission geometry and using the triangular function. The source was  $^{57}\text{Co}$  in Rh matrix with an activity of about 925 MBq (25 mCi). The velocity scale and all the data are referred to metallic  $\alpha$ -Fe absorber at 300K. The absorption spectra were computer fitted by using the WNORMOS-SITE program [20].

### 3. RESULTS AND DISCUSSION

#### 3.1 Weight loss tests

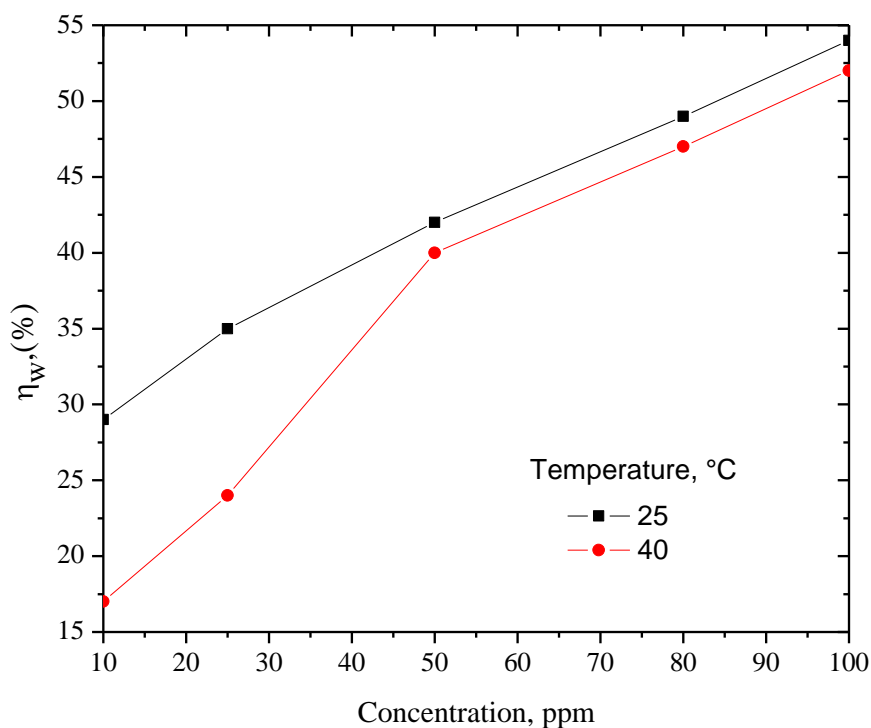


**Figure 1.** Corrosion inhibitor efficiency of AMT for CS 1018 in 1.0 M  $\text{H}_2\text{SO}_4$  as a function of concentration and temperature

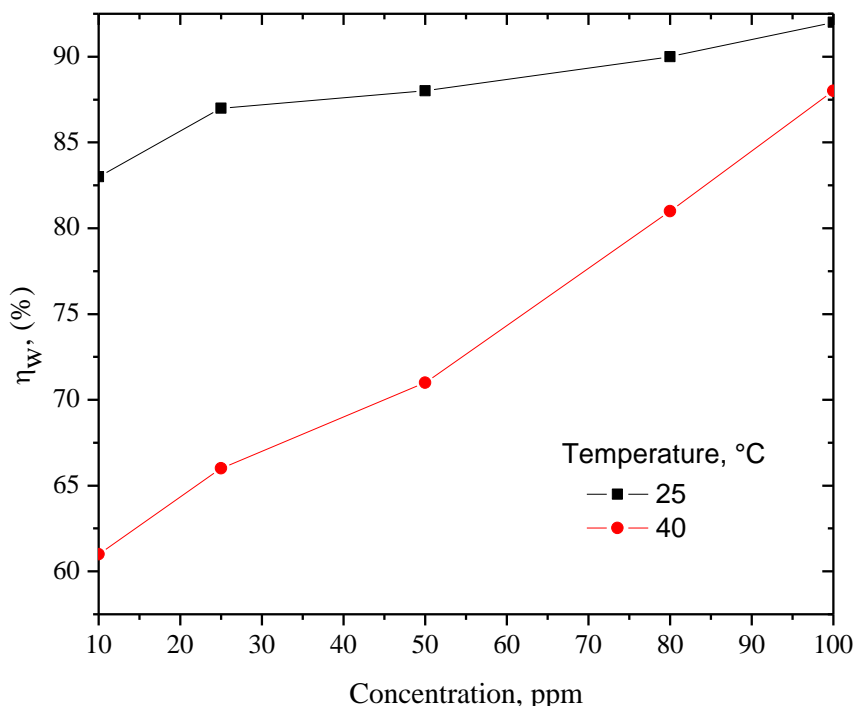


**Figure 2.** Corrosion inhibitor efficiency of AHT for CS 1018 in 1.0 M H<sub>2</sub>SO<sub>4</sub> as a function of concentration and temperature

Figures 1 and 2 show the behavior of the inhibition efficiency ( $\eta_w$ ) calculated from weight loss of the metallic samples, subjected to different inhibitor concentrations, and at temperatures of 25 and 40 °C. The  $\eta_w$  values were calculated using equation (1) as shown below [ 21].

$$\eta_w = \left[ 1 - \frac{W_{cor}}{W_{cor}^o} \right] 100 \tag{1)}$$

where  $W_{cor}$  and  $W_{cor}^o$  are the weight losses in the presence and absence of inhibitor, respectively.

These figures show the variation of  $\eta_w$  against concentration for the AMT and AHT inhibitors, where the greater the concentration, the higher the efficiency; for instance, the efficiencies were 54 and 92% at 25 °C, and 52 and 88% at 40 °C for AMT and AHT inhibitors, respectively, both at 100 ppm. Similar efficiencies were obtained for the AET, APrT, AUT, ATT compounds as shown in Table 2. A common feature among these results is a minor adsorption capacity by inhibitor molecules on the metal surface at 40 °C, indicating that at this temperature the oxidation/reduction processes (corrosion) on the metal surface are faster than the adsorption velocity of inhibitor molecules at the active sites of the metal surface that would prevent its corrosion [13, 22]. Table 2 also shows that the tendency of  $\eta_w$  values against C (inhibitor concentration) slightly deviate from linear relationships as shown in Figs. 1 and 2, indicating a slightly different adsorbing process of inhibitor molecules on the metal surface. In spite of this, these tendencies suggest that the larger the number of used inhibitor molecules, the larger the number of occupied active sites, protecting in this way the metal surface from corrosion.

Additionally, data in Table 2 show the corrosion inhibition effect of all compounds evaluated at temperatures of 25 and 40 °C.

**Table 2.** Weight loss measurements: Inhibition efficiency for CS 1018 in presence of different inhibitors in 1.0 M H<sub>2</sub>SO<sub>4</sub> at temperature of 25 and 40 °C.

Compound	Concentration, mM	Temperature, °C	
		25	40
		Inhibition efficiency, $\eta_w$ , %	
<b>AMT</b>	<b>10</b>	<b>29</b>	<b>17</b>
	25	35	24
	50	42	40
	80	49	47
	100	54	52
<b>AET</b>	10	55	46
	25	58	50
	50	65	54
	80	69	58
	100	73	60
<b>APrT</b>	10	45	35
	25	51	42
	50	71	64
	80	75	75
	100	83	79
	10	83	61
	25	87	66
<b>AHT</b>	50	88	71
	80	90	81
	100	92	88
	10	66	26
	25	71	33
<b>AUT</b>	50	79	46
	80	84	58
	100	88	67
		10	63
	25	75	63
<b>ATT</b>	50	79	75
	80	84	77
	100	87	79

Looking at the  $\eta_w$  values for the lowest and highest compound concentrations (10 and 100 ppm) for 25 °C, the following relations hold: AMT<APrT<AET<ATT<AUT<AHT and AMT<AET<APrT<ATT<AUT<AHT, respectively. Similarly, for the 40 °C sets, the following relations hold: AMT<AUT<APrT<AET<ATT<AHT and AMT<AET<AUT<APrT=ATT<AHT,

respectively. These relations confirm that the size of the aliphatic chains and their location at the molecular structure of the inhibitor is of paramount importance. Such variables (molecular size and volume) may determine the inhibitor adsorption mechanism on the metal surface [8, 11, 17, 19]. Similar observations were reported while evaluating the adsorption properties of imidazoline, amide, amine and amino acids with different aliphatic chain, where the inhibition efficiency is also molecular size dependent [23, 24].

### 3.2 Potentiodynamic polarization

Present inhibition efficiency determinations report relative errors of about ±4 %, which are in good agreement with other studies [7, 25, 26]. Because of this, only three inhibitors were evaluated by Tafel polarization tests, and they were carried out using the AMT, AHT and ATT compounds, which are the most representative by the weight loss analysis. The Tafel polarization measurements for CS 1018 in 1.0 M H<sub>2</sub>SO<sub>4</sub>, in absence and presence of AMT and ATT are shown in Figures 3 and 4, respectively. Similar polarization curves were obtained for the AHT compound. The values of the corrosion current density (*i<sub>corr</sub>*) and corrosion potential (*E<sub>corr</sub>*), as well as the cathodic and anodic Tafel slopes (*β<sub>c</sub>*, *β<sub>a</sub>*) were obtained by the linear extrapolation of the Tafel slopes. Table 3 shows these values as well as the inhibition efficiency (*IE*) that was calculated by equation (2).

$$IE = \left[ \frac{i_{corr} - i'_{corr}}{i_{corr}} \right] 100, \tag{2)}$$

where *i<sub>coo</sub>* and *i' <sub>corr</sub>* are corrosion current densities, with and without corrosion inhibitor, respectively. These figures show that the anodic and cathodic reactions occurring on the metal surface are inhibited by the presence of the corrosion inhibitors AMT and ATT, which are present in the aqueous acid solution. The corrosion potential is shifted to lower values at the highest inhibitor concentrations.

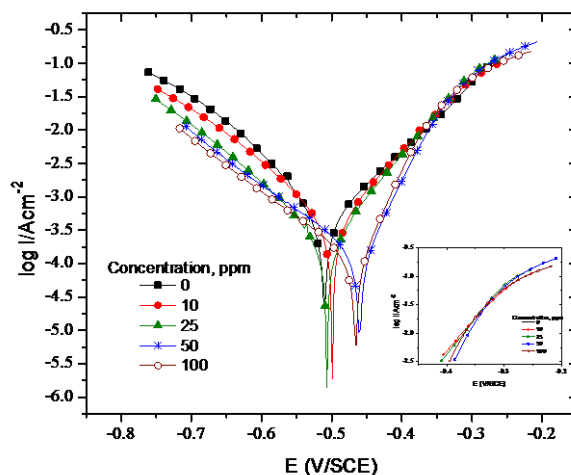


**Figure 3.** Polarization curve for CS 1018 in the presence and absence of different concentrations of compound AMT.

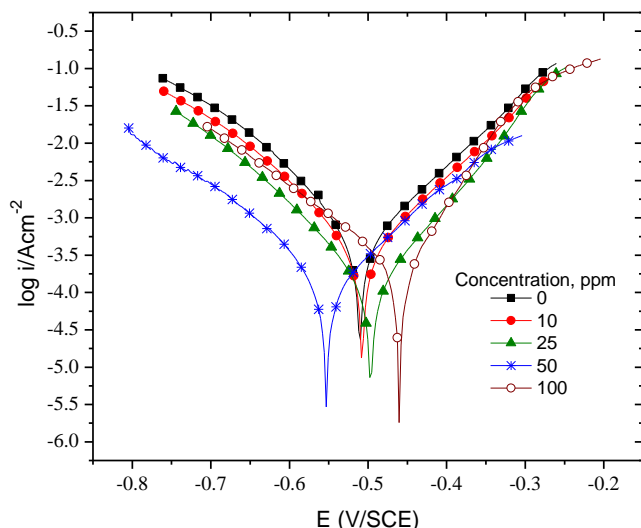


**Figure 4.** Polarization curve for CS 1018 in the presence and absence of different concentrations of compound ATT.

**Table 3.** Electrochemical polarization parameters for CS 1018 in 1.0 M H<sub>2</sub>SO<sub>4</sub> at different concentrations of corrosion inhibitors and 25 °C.

Inhibitor	Concentration (ppm)	$-E_{corr}$ (mV/SCE)	$i_{corr}$ ( $\mu\text{A}/\text{cm}^2$ )	$\beta_a$ (mVdec <sup>-1</sup> )	$\beta_c$ (mVdec <sup>-1</sup> )	IE, %
<b>Blank</b>	-	511	1863	124	108	
<b>AMT</b>	10	508	890	104	97	31
	25	504	846	92	94	40
	50	490	507	78	89	48
	100	492	359	82	87	54
<b>AHT</b>	10	499	969	91	102	77
	25	507	706	79	101	82
	50	468	434	75	153	84
	100	466	285	87	103	89
<b>ATT</b>	10	508	995	115	107	57
	25	497	663	111	109	72
	50	553	517	123	115	74
	100	461	217	75	118	85

Cathodic polarization curves also show parallel lines with the inhibitor concentration with respect to the polarization curve of the blank. This behavior in the cathodic process, suggests that the addition of the corrosion inhibitor in the corrosive medium does not modify the mechanism of reduction of protons, and that the reaction is only controlled by the activation energy. This also suggests that once the inhibitor compound is adsorbed on the metal surface, it blocks off the active sites. Under these circumstances, the available metal surface (1-θ) for free H<sup>+</sup> ions is reduced, while the reaction mechanism is not affected [14, 15]. According to the polarization curves of the anodic side and their respective β<sub>a</sub> values (Table 3), the inhibitor concentration has an effect on the reaction



mechanism, reducing the dissolution speed of the metal by forming a protective film and decreasing the number of active sites and  $\text{SO}_4^{2-}$  ions. However, a peculiar process was observed in the anodic branch of the polarization curve of the AMT compound. The current in the presence of this inhibitor is higher than that of the blank in the potential ranging from - 353 to - 287 mV (Figure 3); this process may be attributed to a desorption process of the inhibitor from the metal surface. Some authors have defined this process as a desorption process occurring at the potential ( $E_d$ ), a process that will be affected by the presence of corrosion iron products of low solubility (like melanterite, rosenite, szomolnokite, etc), oxyhydroxides (goethite) and steel impurities (e.g.,  $\text{Fe}_3\text{C}$ ), which together impede the formation of a passive surface film [26]. Moreover, data in Table 3 show that the presence of the AMT compound causes a change in the ( $E_{corr}$ ) at the anodic direction with a potential difference of 21 mV with regard to that of the blank; while for the AHT compound, it was 45 mV. However, the ATT compound presents shifts of 50 mV to the anodic side and 42 mV in the cathode side with respect to the ( $E_{corr}$ ) of the blank. This process may be attributed to the change of adsorption behavior of the compounds on the metal surface, while increasing the inhibitor concentration. These shifts are of considerable importance because some studies classify the type of inhibitor with respect to ( $E_{corr}$ ) of the blank. If the shift of the  $E_{corr}$  values in the presence of corrosion inhibitor is greater than 85 mV, the compound is an inhibitor of anodic type and vice versa, i. e. if the shift is lower than 85 mV, the inhibitor belongs to the cathodic type [27]. Therefore, compounds evaluated as corrosion inhibitors are usually classified as mixed type inhibitors. For instance, whereas the AMT and AHT compounds operate on the anodic side, the ATT compound operates on both sides, i. e. on the anodic and cathodic sides. This indicates that the potential on the surface of the electrode will define the characteristics of the inhibitor and its adsorption mechanism. The values of  $i_{corr}$  linearly decrease as the inhibitor concentration increases (Table 3), indicating an inhibition process. According to the slope values ( $\beta_c$  and  $\beta_a$  given in Table 3) and the behavior of the Tafel polarization curves (Figures 3 and 4), the influence of the molecule structure is relevant for ruling the aliphatic chain size. The aliphatic chain will define if the protective film is more uniform than any other resulting from other inhibitor compounds of different size. The interaction between the inhibitor molecules and the iron metal surface occurs only through the TDZ ring and the  $-\text{NH}_2$  group, where the electronic density is higher than in any other part of the molecule [12]. A second structure factor or structure variable that predetermines a higher or lower inhibition efficiency may be the size of the aliphatic chain, suggesting that its final orientation, relative to the corrosive medium, is important. This and its molecular volume will define the properties of the protective layer of the inhibitor. Generally speaking, steric hindrance from large molecules will limit the anticorrosive process.

### 3.3 Adsorption isotherm

Namely, corrosion protection by inhibitors is the result of the adsorption of an organic inhibitor in the metal/solution interface. This adsorption process forms a monolayer made of inhibitor molecules, which ideally will prevent the metal surface from being attacked by acids, i. e., avoiding corrosion. When the inhibitor has a poor affinity to the metal surface, electrically charged, the

corrosion process begins at the active metal surface sites [10, 22]. In order to understand the physical process of adherence of molecules on the metal surfaces, one brings about the concepts of physical adsorption and adsorption isotherms. Thus, different adsorption isotherms were analyzed in order to obtain information about the interactions between TDZ derivatives and the metal surface. The best fit to the experimental isotherms was obtained using the Langmuir equation (3).

$$\frac{C_{inh}}{\theta} = \frac{1}{K_{ads}} + C_{inh} \tag{3}$$

where  $C_{inh}$  is the inhibitor concentration at equilibrium,  $\theta$  is the occupied fractional surface area and  $K_{ads}$  is the Langmuir adsorption constant at equilibrium. The  $\theta$  values were calculated from the weight loss data using the following equation (4)

$$\theta = \left( \frac{W_0 - W_{Cl}}{W_0} \right) \tag{4}$$

where  $W_0$  and  $W_{Cl}$  are the weight loss corrosion rates of CS 1018 in the absence and presence of inhibitor.

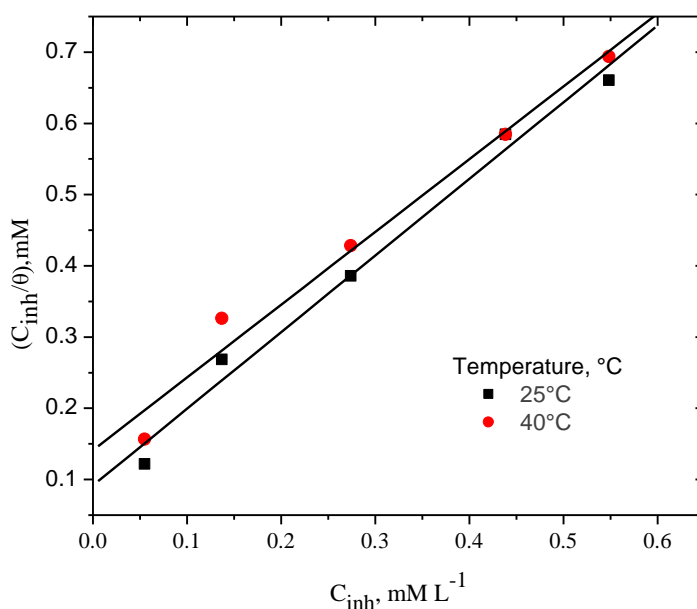


**Figure 5.** Langmuir isotherm adsorption model of APt on the CS 1018 surface in 1.0 M H<sub>2</sub>SO<sub>4</sub>.

This isotherm is based on the assumption that all adsorption sites are equivalent and that particle binding occurs independently from nearby sites either being occupied or not [27, 28]. A plot of  $C_{inh}/\theta$  against  $C_{inh}$  shows a straight line with slope equal to one, indicating that the adsorption follows the Langmuir adsorption isotherm as shown in Figs. 5-7. The adsorption equilibrium constant,

$K_{ads}$ , obtained from the Langmuir adsorption isotherm is related to the standard free energy of adsorption ( $\Delta G_{ads}^0$ ) for equation (5):

$$\Delta G_{ads}^0 = -RT \ln(55.5K_{ads})$$

5)

where  $R$  is the universal gas constant,  $T$  the temperature and the value of 55.5 is the molar concentration of water in the solution.

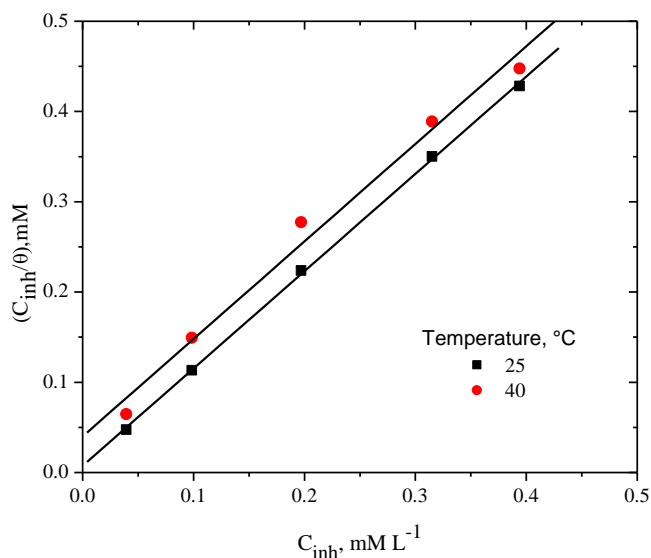


**Figure 6.** Langmuir isotherm adsorption model of AHT on the CS 1018 surface in 1.0 M H<sub>2</sub>SO<sub>4</sub>.

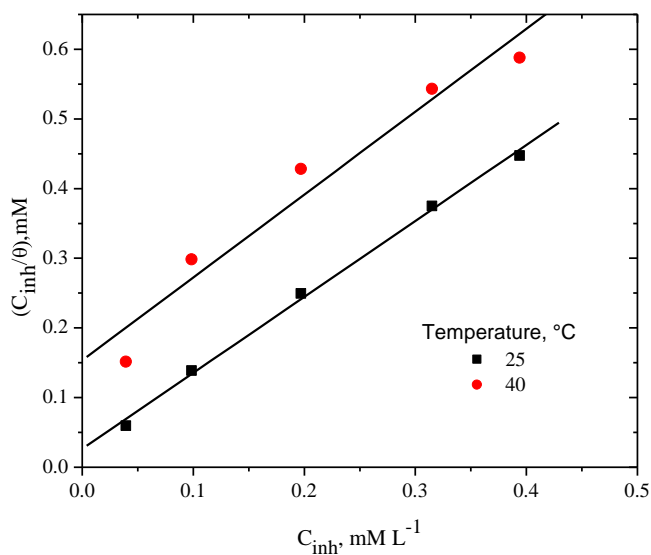


**Figure 7.** Langmuir isotherm adsorption model of AUT on the CS 1018 surface in 1.0 M H<sub>2</sub>SO<sub>4</sub>.

**Table 4.** Calculated thermodynamic parameters from Langmuir adsorption isotherm

Inhibitor	Temperature (°C)	R <sup>2</sup>	K <sub>ads</sub> (mol <sup>-1</sup> )	-ΔG <sub>ads</sub> <sup>0</sup> (kJ mol <sup>-1</sup> )
AMT	25	0.98	5.51	14.19
	40	0.97	2.62	12.97
AET	25	0.99	19.53	17.32
	40	0.99	18.66	18.08
APrT	25	0.99	10.89	15.88
	40	0.98	7.08	15.55
AHT	25	0.99	33.33	22.08
	40	0.99	25.06	18.84
AUT	25	0.99	48.54	19.58
	40	0.95	8.35	15.98
ATT	25	0.99	60.61	20.13
	40	0.99	45.45	20.39

The high values of  $K_{ads}$  and negative values of  $\Delta G_{ads}^0$  suggest a fast adsorption of the TDZ derivatives on the metal surface (Table 4). As a result of this adherence of TDZ molecules on the metal surface, the available surface area to develop oxidation reactions is so reduced that less water molecules interact with the active sites of the metal. In addition to this, the stability of the corrosion products and the inhibitor itself are important to be considered. A comparison of the  $\theta$  values reported in Table 2 shows that the stability of the inhibitor layer is reduced by incrementing its temperature (T); that is, the  $\theta$  values for 40 °C are lower than those for 25 °C. A desorption process of inhibitor is produced from the metal surface at higher temperatures than at room temperature. Such a process may occur in two ways: (i) a fast formed aggregate of corrosion products (Rhomboclase, Szomolnokite, Goethite, etc.) on the metal surface may disturb the stability of the inhibitor layer due to the fact that the kinetic oxidation reaction may be promoted while increasing T; (ii) the desorption velocity of the inhibitor on the metal surface is faster than its adsorption while increasing T. The stability of the inhibitor layer keeps a close relation with the electrical charge on the metal surface which increases with T. As a result, an inverse relation appears between  $\theta$  and T, as reported here and by other authors [13, 22].

By taking into account the aforementioned discussion, it may be concluded that the inhibition process of these TDZ derivatives on the CS 1018 in 1.0 M H<sub>2</sub>SO<sub>4</sub> only has a physical character due to a weak electrostatic attraction between the inhibitor and the metal surface.

### 3.4 SEM analysis

Figure 8 (a through d) shows the SEM images of CS 1018 surface before and after, exposed to an open circuit potential (OCP) for 24 h at 25 °C in the acidic test solution, in absence and presence of corrosion inhibitors. Figure 8 (a) shows CS 1018 surface used, where a homogeneous topography and well oriented lines, due to the mechanical preparation of the samples, are observed. On the other hand,

the SEM image of a attacked CS 1018 sample, subjected to electrochemistry tests (OCP), Fig. 8 (b), shows considerable surface damage together with a slight indication of localized corrosion (as indicated with arrows).

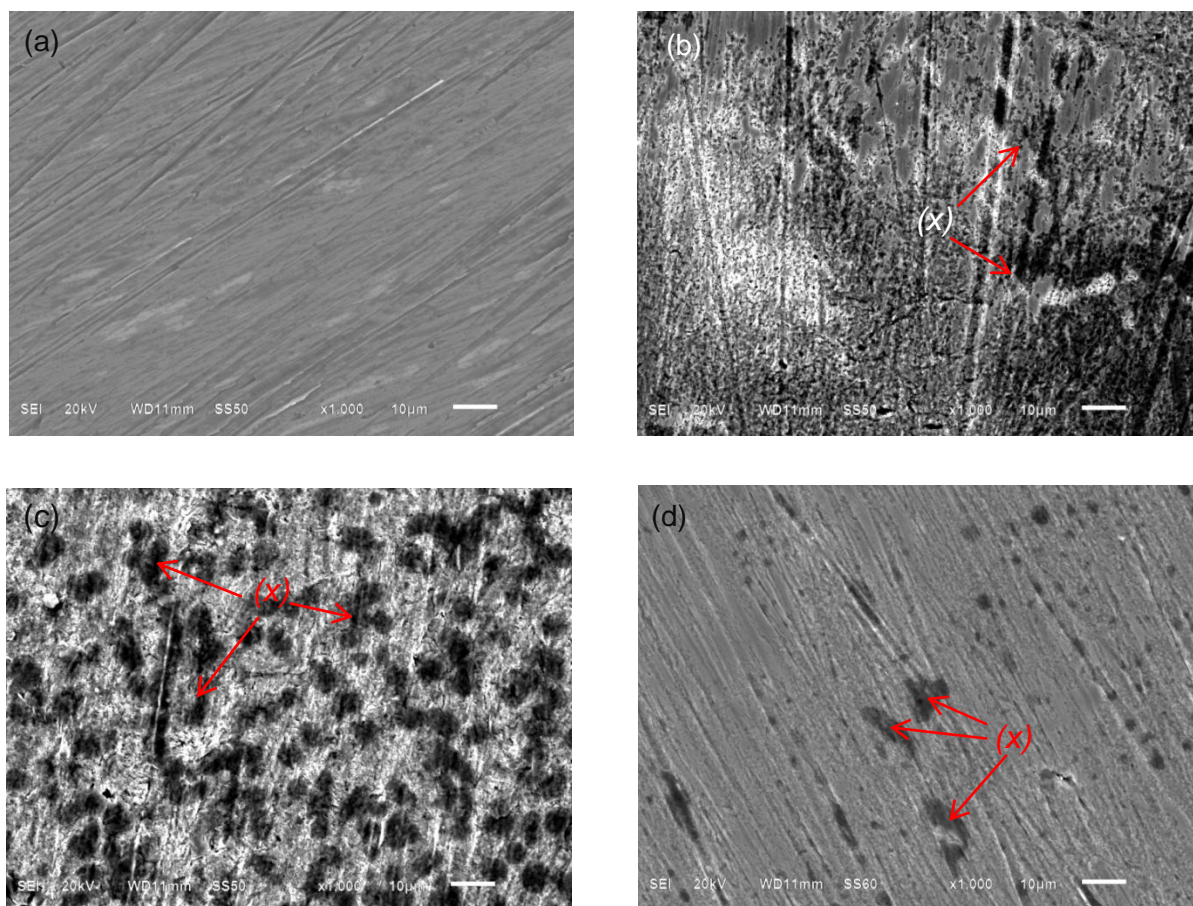


**Figure 8.** SEM image CS 1018 surface: (a) before electrode polarization, (b) in 1.0 M  $\text{H}_2\text{SO}_4$  after 24 h, (c) and (d) inhibited in 1.0 M  $\text{H}_2\text{SO}_4$  with 100 ppm of AMT and AHT after 24 h.

This local corrosion may arise from metal dissolution as a result of anodic reaction. The corresponding image of a CS 1018 sample, subjected to the same tests, which was referred to above, but in the presence of less efficient AMT inhibitor (at 100 ppm), Fig. 8 (c), displayed a damage, showing a homogeneous distribution of large dark marks, associated with the corrosion process. According to Fig. 8 (c), a larger surface area is corrosion free and/or covered by the AMT inhibitor. Finally, the image corresponding to the CS 1018 surface treated with the most efficient AHT inhibitor, (Table 2), is displayed in Fig. 8 (d). This image shows an almost clean surface area, few dark points are observed, indicating local damage. The rest of the image shows similar features to those of the untreated sample (Fig. 8 (a)), indicating that the AHT inhibitor largely reduces the current density of active sites on the metallic surface, where the oxidation/reduction process takes place.

## 3.5 XRD results

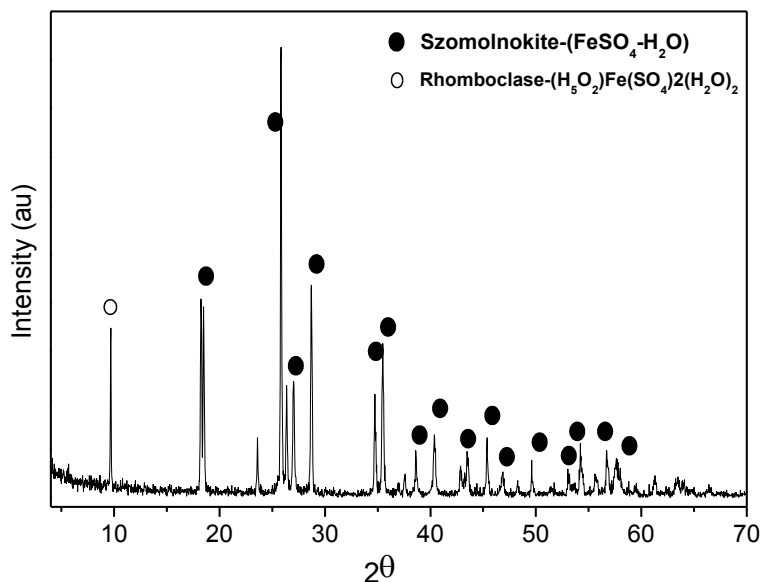


**Figure 9.** XRD pattern shows two characteristic corrosion products formed in the presence of AUT.

The nature of the corrosion products, obtained in the present work, was analyzed by their corresponding XRD patterns, and Fig. 9 shows a pattern that is characteristic for all the studied corrosion products. As indicated by the dark circles in this figure, most of the diffracted lines correspond to those of the Zsomolnokite phase ( $\text{Fe}_2\text{SO}_4 \cdot \text{H}_2\text{O}$ ), i. e., monohydrated iron sulfate. Most of the diffracted peaks match those of the JCPDS No 81-0019 card. Additional peaks of minor intensity appear in this pattern (Fig.9). The main of these (indicated by an open circle) appears at  $2\theta = 9.6^\circ$ , and can be assigned, according to the JCPDS No. 70-1820 card, to the Rhomboclase phase.

## 3.6 Mössbauer results

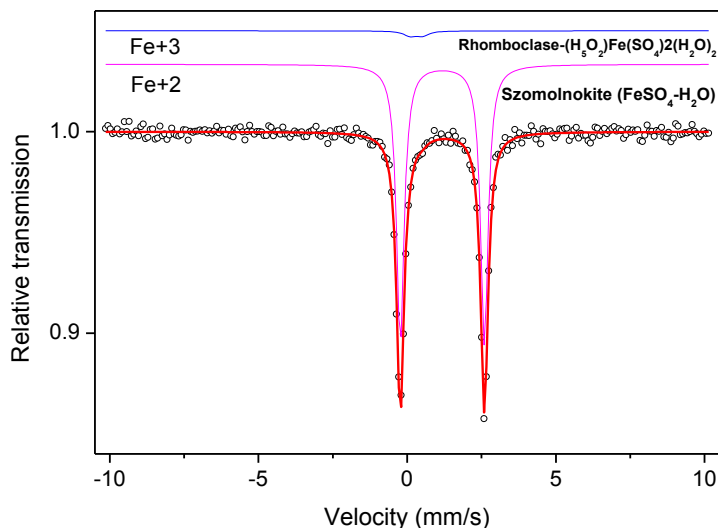


**Figure 10.** Mössbauer spectrum of a characteristic corrosion product formed in the presence of AUT.

**Table 5.** Mössbauer parameters take at 300 K

Sample	Phase	$\delta$ (mm/s)	$\Delta$ (mm/s)	Relative Area (%)
AMT	Szomolnokite	1.18	2.81	96.1
	Rhomboclase	0.22	0.43	3.9
AET	Szomolnokite	1.17	2.77	98.0
	Rhomboclase	0.43	0.30	2.0
APrT	Szomolnokite	1.17	2.79	96.7
	Rhomboclase	0.20	0.30	3.3
AHT	Szomolnokite	1.17	2.79	93.5
	Rhomboclase	0.19	0.30	6.5
AUT	Szomolnokite	1.18	2.82	97.3
	Rhomboclase	0.30	0.41	2.7
ATT	Szomolnokite	1.17	2.79	96.5
	Rhomboclase	0.30	0.26	3.5

Key:  $\delta$  = isomer shift given relative to  $\alpha$ -Fe at RT;  $\Delta$  = quadrupole splitting; Error:  $\delta = \pm 0.01$  mm/s;  $\Delta = \pm 0.01$  mm/s.

Additional information on the nature of these corrosion products can be obtained by Mössbauer spectroscopy (MS). In this sense, Fig.10 also shows a typical Mössbauer spectrum of these products. The Mössbauer spectrum consists of a pattern that is simpler than the XRD one. It contains two doublets indicating the presence of two iron sites or phases. The isomer shifts ( $\delta$ ) of these doublets relative to that of  $\alpha$ -Fe are 1.18 and 0.30 mm/s, and their corresponding quadruple splitting ( $\Delta$ ) are 2.82 and 0.41 mm/s, respectively. The Mössbauer parameters with the high values correspond to Szomolnokite phase [29-31]; and those parameters ( $\delta$  and  $\Delta$ ) with the lower values correspond to the Rhomboclase phase [31]. Both techniques, XRD and MS, are in good agreement with the nature of the (intermediate) corrosion products (i. e., the Szomolnokite and Rhomboclase phases corrosion products). It is worth noticing from the data in Table 5 that whereas the Mössbauer parameters of the Szomolnokite phase vary within that standard deviation of the data, those parameters of the Rhomboclase phase do vary in a systematic way quite above the standard deviations among the different samples. It is suggested that this variations could arise from a different hydration of the Rhomboclase phase, which is a mineral species of the coquimbite ( $\text{Fe}_2(\text{SO}_4)_3 \cdot 9\text{H}_2\text{O}$ ) [30, 31]. It can be concluded from the XRD and MS results that the formation of iron oxides under the present experimental conditions were not formed, and only intermediate corrosion products were detected (the Szomolnokite and Rhomboclase phases).

### 3.7 Inhibition mechanism

The steel surface in acidic medium contains anodic and cathodic sites on which the simultaneous electrochemical reactions of iron oxidation and hydrogen evolution take place, respectively (Fig. 11). It is assumed that  $\text{FeSO}_4$  covers a considerable portion of the metal surface, leaving less available space for organic molecules to be adsorbed.



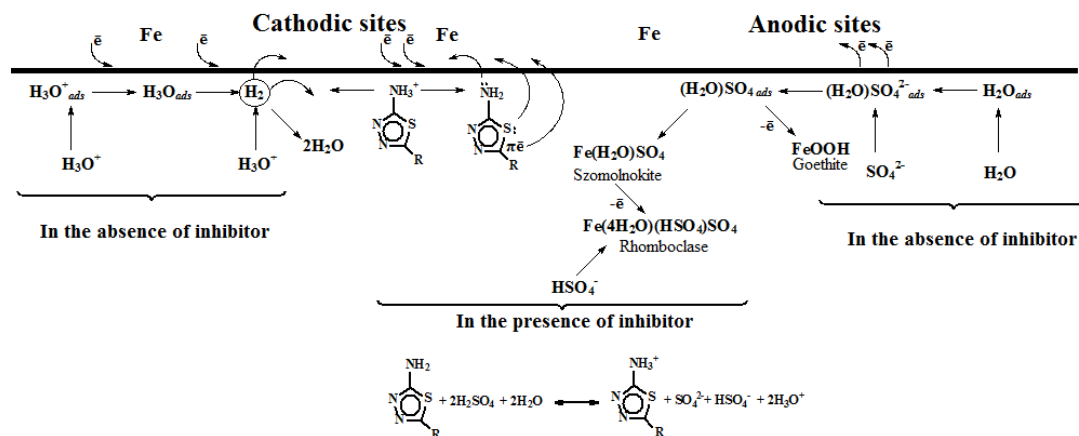


**Figure 11.** Corrosion inhibition mechanism and adsorption model of thiadiazole compounds on iron surface in aqueous sulfuric acid medium.

On the cathodic sites, the CI seems to work in the following way: the cationic form, which was formed by protonation of the amino group of TDZ in contact with an aggressive environment, is adsorbed on the metallic surface through Van der Waals forces; in this way, a physical barrier is formed to prevent the adsorption of hydronium ions ( $\text{H}_3\text{O}^+$ ), decreasing the hydrogen evolution. Later, the cationic form of TDZ accepts electrons from the metallic surface to reach electroneutrality [32]. These TDZ forms contain  $\pi$  electrons of aromatic ring, sulfur and nitrogen atoms with a free electron pair available to be donated to the metallic surface; in this way, chemisorption occurs by a retro-donation mechanism and a layer is deposited on the metallic surface to be protected from corrosion. In addition, the hydrophobic chains help the displacement of water molecules from the metal surface. In this way, on the anodic sites, in the absence of CI, metal dissolution occurred and corrosion products such as Goethite evolved. According to our previous research, Goethite was formed in the sulfuric acid media in the absence of CIs; however, in the presence of the ionic liquid type CIs, iron sulfates such as Melanterite and Rozenite were formed [27, 33]. In this work, the corrosion process, with the presence of TDZ type CI, is significantly mitigated; this is attributable to the formation of a CI film, which probably recovers the hydrated iron sulfate, like Szomolnokite  $\text{Fe}(\text{H}_2\text{O})\text{SO}_4$ , which is one of the intermediate corrosion products. Unlike Szomolnokite, Melanterite  $\text{Fe}(\text{H}_2\text{O})_7\text{SO}_4$  and Rozenite  $\text{Fe}(\text{H}_2\text{O})_4\text{SO}_4$  contain more water molecules in their structure, which can be explained by the micellar nature of the ILs. Szomolnokite leads to the oxidation of species, which is slowed down and only can yield Rhomboclase species  $\text{Fe}(\text{H}_2\text{O})_4(\text{HSO}_4)\text{SO}_4$ , but not Goethite. These reaction routes are in good agreement with the corrosion product, which was shown by the XRD and Mössbauer analyses.

Additionally, the size of aliphatic chains had an effect on the CI as the inhibitor efficiency was in the order  $\text{AMT} < \text{APrT} < \text{AET} < \text{ATT} < \text{AUT} < \text{AHT}$ , to be the most efficient CI rather than with 7 carbon atoms. This effect is apparently attributable to either a lack of geometric length and form of CI molecules or net space occupied by the hydrocarbon chain because long alkyl chains with more than ten carbon atoms can fold the spacer of the tail [33].



#### 4. CONCLUSIONS

The results of the gravimetric tests concerning the thiadiazole derived compounds evaluated as steel AISI 1018 inhibitors in 1.0 M H<sub>2</sub>SO<sub>4</sub> show that their efficiency is a function of their concentration and temperature.

The Tafel polarization tests confirmed that these compounds hinder the dissolution of SC 1018 in 1.0 M H<sub>2</sub>SO<sub>4</sub> and that these compounds are mixed-type inhibitors.

The  $K_{ads}$  and  $\Delta G_{ads}^0$  values indicate that the adsorption process of the compounds on the metal surface is performed through a physical adsorption process; i.e. by means of electrostatic interactions.

The efficiency results confirm the importance of the aliphatic chain in the molecule structure; as a consequence, it can be concluded that in these compounds there is an optimum length for the aliphatic chain, which was obtained for the AHT compound with  $R = C_7H_{15}$ .

#### ACKNOWLEDGMENT

O.O.-X. thanks SNI, PROMEP/03.5/11/6848 and VIEP

#### References

1. C.F. James, V.S. Ranjani, W.S. Jr. Robert, *Ind. Eng. Chem. Res.*, 51 (2012) 5273.
2. R.C. Mahbuboor, H. Ming-Kai, D.V. Radisav, A.D. David, *Ind. Eng. Chem. Res.*, 51 (2012) 4230.
3. N. Muthukumar, A. Ilangovan, S. Maruthamuthu, N. Palaniswamy, *Electrochim. Acta.*, 52 (2007) 7183.
4. R. Aruliah, M. Sundaram, T. Yen-Peng, *Ind. Eng. Chem. Res.*, 47 (2008) 6925.
5. T. Zhihua, Z. Shengtao, L. Weihua, H. Baorong, *Ind. Eng. Chem. Res.*, 49 (2010) 2593.
6. V.S. Sastri, *Corrosion Inhibitors Principles and Application*; John Wiley & Sons: New York, (1998).
7. M. El Azhar, B. Mernari, M. Traisnel, F. Bentiss, M. Lagrenée, *Corros. Sci.*, 43 (2001) 2229.
8. M.A. Quraishi, S. Khan, *J. Appl. Electrochem.*, 36 (2006) 539.
9. Y.M. Tang, W.Z. Yang, X.S. Yin, Y. Liu, R. Wan, J.T. Wang, *Mater. Chem. Phys.*, 116 (2009) 479.
10. F. El-Taib Heakal, A.S. Fouda, M.S. Radwan, *Mater. Chem. Phys.*, 125 (2011) 26.
11. T.T. Qin, J. Li, H.Q. Luo, M. Li, N.B. Li, *Corros. Sci.*, 53 (2011) 1072.
12. Y. Tang, X. Yang, W. Yanga, R. Wan, Y. Chen, X. Yin, *Corros. Sci.*, 52 (2010) 1801.
13. A.K. Singh, M.A. Quraishi, *Corros. Sci.*, 52 (2010) 1373.
14. R. Solmaz, *Corros. Sci.*, 52 (2010) 3321.
15. Döner, R. Solmaz, M. Özcan, K. Gülfeza, *Corros. Sci.*, 53 (2011) 2902.
16. E.M. Sherif, P. Su-Moon, *Electrochim. Acta.*, 51 (2006) 6556.
17. Y. Tang, X. Yang, W. Yang, Y. Chen, R. Wan, *Corros. Sci.*, 52 (2010) 242.
18. X. Joseph Raj, N. Rajendran, *Int. J. Electrochem. Sci.*, 6 (2011) 348.
19. F. El-Taib Heakal, A.S. Fouda, M.S. Radwan, *Int. J. Electrochem. Sci.*, 6 (2011) 3140.
20. R.A. Brand, *Nucl. Instr. Meth. B.*, 28 (1987) 398.
21. E.A. Flores, O. Olivares, N.V. Likhanova, M.A. Domínguez-Aguilar, N. Nava, D. Guzman-Lucero, M. Corrales, *Corros. Sci.*, 53 (2011) 3899.
22. W. Chen, H.Q. Luo, N.B. Li, *Corros. Sci.*, 53 (2011) 3356.
23. V. Jovancicevic, S. Ramachandran, P. Prince, *Corrosion* 55 (1999) 449.
24. A.A. Aksüt, S. Bilgiç, *Corros. Sci.*, 33 (1992) 379.

25. M.A. Migahed, H.M. Mohamed, A.M. Al-Sabagh, *Mater. Chem. Phys.*, 80 (2003) 169.
26. M.A. Amin, M.M. Ibrahim, *Corros. Sci.*, 53 (2011) 873.
27. N.V. Likhanova, M.A. Dominguez-Aguilar, O. Olivares-Xometl, N. Nava-Entzana, E. Arce, H. Dorantes, *Corros. Sci.*, 52 (2010) 2088.
28. A.K. Satapathy, G. Gunasekaran, S.C. Sahoo, K. Amit, P.V. Rodrigues, *Corros. Sci.*, 51 (2009) 2848.
29. N.V. Likhanova, O. Olivares-Xometl, D. Guzmán-Lucero, M.A. Domínguez-Aguilar, N. Nava, M. Corrales-Luna, M.C. Mendoza, *Int. J. Electrochem. Sci.*, 6 (2011) 4514.
30. Y. Rothstein, M.D Dyar, M.W. Schaefer, M.D. Lane, J.L. Bishop, 36th Annual Lunar and Planetary Science Conference, March 14–18, League City, Texas, abstract No. 2108, 2005.
31. Vanessa A. O'Connor, Thesis, Faculty Adviser Melinda Darby Dyar, Ph.D., Supervisor, Mount Holyoke College, (2005)
32. M. Palomar-Pardavé, M. Romero-Romo, H. Herrera-Hernández, M.A. Abreu-Quijano, Natalya V. Likhanova, J. Uruchurtu, J.M. Juárez-García, *Corros. Sci.*, 54 (2012) 231.
33. N.A. Negm, S.M.I. Morsy, *J. Surfactants. Deterg.*, 8 (2005) 283.